Targeted AKT inhibition in prostate cancer cells and spheroids reduces aerobic glycolysis and generation of hyperpolarized [1-^{13}C] lactate

Sui Seng Tee[1], Izabela Suster, Steven Truong[2], Sangmoo Jeong[1], Roozbeh Eskandari[1], Valentina DiGialleonardo[1], Julio A. Alvarez[3], Hannah N. Aldeborgh[1], Kayvan R. Keshari[1,3]*

[1]Department of Radiology and Molecular Pharmacology Program, Memorial Sloan Kettering Cancer Center, New York, NY 10065, USA
[2]Hunter College, New York, NY 10065, USA
[3]Weill Cornell Medical College, NY 10065, USA
*Corresponding Author:

Kayvan R. Keshari, Ph.D.
Assistant Member
Department of Radiology and Molecular Pharmacology Program
Memorial Sloan Kettering Cancer Center
1275 York Avenue
New York, NY 10065
Phone: (646) 888-3631
Fax: (646) 422-0247
rahimikk@mskcc.org

Running title: Hyperpolarized MRS in spheroids

Key words: 3D culture, Metabolic imaging, Pyruvate, Metabolism, Kinetics

Financial Support: This research was funded in part through the NIH/NCI Cancer Center Support Grant P30 CA008748 (K.R. Keshari), NIH/NCI R01 CA195476 and NIH/NIBIB R00 EB014328 (K.R. Keshari) as well as Memorial Sloan Kettering's Center for Molecular Imaging and Nanotechnology (CMINT) (S.S. Tee).

Abstract

The PI3K/AKT/mTOR (PAM) signalling pathway is frequently mutated in prostate cancer. Specific AKT inhibitors are now in advanced clinical trials and this study investigates the effect of MK2206, a non-ATP competitive inhibitor, on the cellular metabolism of prostate cancer cells. We observed a reduction in cell motility and aerobic glycolysis in prostate cancer cells with treatment. These changes were not accompanied by a reduction in the ratio of high-energy phosphates or a change in total protein levels of enzymes and transporters involved in glycolysis. However, a decreased ratio of NAD+/NADH was observed, motivating the use of hyperpolarized magnetic resonance spectroscopy (HP-MRS) to detect treatment response. Spectroscopic experiments were performed on tumor spheroids, 3D structures that self-organize in the presence of an extracellular matrix. Treated spheroids showed decreased lactate production with on-target inhibition confirmed using immunohistochemistry, demonstrating that HP-MRS can be used to probe treatment response in prostate cancer spheroids and can provide a biomarker for treatment response.

Introduction

Prostate cancer affects one in six men in the Western world and one in six of those diagnosed with prostate cancer die of metastatic castration-resistant prostate cancer (CRPC)(1). Currently, only six non-hormonal therapeutics have been shown to prolong survival, highlighting the crucial need uncover alternative drug targets for CRPC as well as non-invasive methods to rapidly evaluate therapeutic response.

The PI3K/AKT/mTOR (PAM) signaling pathway has diverse functions including regulating growth, metabolism and migration(2). Activation of PI3K can be achieved by receptor tyrosine kinases, G-protein-coupled receptors as well as some oncogenes. This leads to the phosphorylation of phosphatidyl-inositol 4,5-bisphosphate (PIP2) to phosphatidyl-inositol 3,4,5-triphosphate (PIP3) and recruitment of AKT to the plasma membrane. The phosphatase PTEN acts as a negative regulator of AKT, inhibiting recruitment of the kinase to the plasma membrane. Activated AKT phosphorylates a host of proteins involved in a range of pro-growth effects, including mTOR(3). mTOR is a serine threonine kinase involved in regulation of cell growth, contingent on availability of nutrients(4). Significantly, this pathway is mutated in 42% of primary and 100% of metastatic prostate cancer(5). Many inhibitors of this pathway are currently being tested in Phase I/II trials for prostate cancer, either in isolation or in combination with conventional chemotherapies(6).

Rapid evaluation of treatment efficacy is crucial, especially in the clinical management of CRPC. Effective assessment of cancer therapy could guide drug selection and molecular

imaging methods such as metabolic imaging have already shown great promise in terms of detecting treatment response in cancer(7). Metabolic imaging is an example of an imaging platform that has the unique ability to detect nutrient utilization (8) in both pre-clinical studies and in patients. The advent of hyperpolarized NMR has greatly increased the sensitivity of detection for ^{13}C NMR(9). Hyperpolarization describes a number of techniques that are used to enhance the polarization of nuclear spins, with dissolution dynamic nuclear polarization (dDNP) being the mostly widely used to study *in vivo* metabolism(8). dDNP is based on polarizing nuclear spins in a frozen sample, where microwave irradiation is used to transfer polarization from an organic free radical to an NMR-active metabolite of interest. Rapid dissolution provides polarized metabolites with greatly enhanced signal-to-noise enabling the detection of metabolic flux *in vivo*(9). First-in-man studies of hyperpolarized (HP) [1-^{13}C] pyruvate have been performed in early-stage prostate cancer patients with no adverse effects and an excellent ability to distinguish malignant and normal prostate, demonstrated by regions of increased generation of HP [1-^{13}C] lactate(10).

While non-invasive imaging of patients will benefit greatly from HP NMR, magnetic resonance spectroscopy in general, enables measurements of cellular physiology and metabolism non-destructively *in situ* and repeatedly with minimal perturbation to cellular physiology (11). This study investigates the possibility of measuring changes in treatment response of prostate cancer cells and spheroids using HP [1-^{13}C] pyruvate after AKT inhibition. While HP experiments have been performed on cell suspensions(12) and sodium alginate encapsulated cells in fluidized bioreactors(13), we believe that the ability to measure metabolic flux in patient-derived tumor organoids or cell line-derived tumor spheroids that are 3D cultures that mimic human disease(14) will allow high-throughput screening of multiple samples with distinct genetic backgrounds. Because these cultures show high-fidelity to clinical disease, prostate cancer organoids have already been used for drug screening (15). This work investigates the possibility of detecting changes in metabolic flux of prostate cancer spheroids after drug treatment, potentially providing complementary information prior to clinical trials and revealing the potential for this approach to be used *in vivo* in patients to annotate successful treatment.

Materials and Methods

Cell culture and growth curve determinations

PTEN-mutated LnCAP and homozygous PTEN-deleted PC3 cell line were obtained from the American Type Culture Collection (ATCC) and cultured in RPMI 1640 (Gibco®) media supplemented with 10% fetal bovine serum (FBS), 2.5mM L-glutamine and incubated at 37°C in 5% CO_2. MK2206, Perifosine and GDC0068 were obtained from Cayman Chemicals (Ann Arbor, MI). Growth curve determination was quantified every 4 hours for a total of 70 hours using an Incucyte (Essen Bioscience, MI) at 10x magnification. IC50 was determined using Prism GraphPad using a nonlinear regression for exponential growth.

Western blotting and immunocytochemistry

Cells were lysed in Pierce RIPA buffer with 100x Halt™ protease and phosphatase inhibitor cocktail (Thermo Fisher, MA). The samples were resolved by 4-12% SDS-PAGE and transferred to nitrocellulose membranes. The blots were blocked with 5% bovine serum albumin, 1% Tween-20 Tris-buffered saline. All primary and secondary antibodies were obtained from Cell Signaling Technology (MA) and visualized using chemiluminescence. For immunocytochemistry, cells were grown on coverslips and fixed with 100% methanol before blocking and incubation with primary antibodies and probed with secondary antibody coupled to Alexa-488 (Thermo Fisher, MA)

Cell tracking and velocity determination

LnCAP cells, treated with MK2206 were incubated at 37°C under a time-lapse bright-field microscope (EVOS, Thermo Scientific, MA). Images of the cells were taken every 30 minutes over a 6-hour period. The images were compiled and quantified manually using the TrackMate application in ImageJ. For every treatment condition, a total of at least 15 individual cells were tracked and velocity measurements were quoted as the mean value ± standard error.

Metabolite determination and fractional enrichment

Extracellular metabolites in cell culture media were directly measured using 1H NMR on a 14.1T NMR spectrometer (Bruker Biospin, Billerica, MA), after addition of 100uL of 10X PBS in D2O, containing 0.5mM DSS as an internal standard and 10mM imidazole as a pH indicator to 100µl of media.

Determination of high-energy phosphates was performed using the ADP/ATP Ratio Assay Kit (Abcam, Cambridge, MA) according to the manufacturer's instructions.

Fractional enrichment experiments were performed as previously described. Briefly, a total of 1 x 10^6 cells were plated in each well of a 6-well plate and treated with either vehicle or MK2206 for 24 hr. Subsequently, the media was exchanged for media containing 5mM [1,6-$^{13}C_2$] glucose enriched media (3 wells) or 5mM non-enriched glucose (3 wells) and incubated for 3 hr. After washing with ice-cold PBS, cells were extracted with 2mL of 80% cold methanol. Extracts were placed at -80°C overnight then centrifuged and the supernatant isolated and lyophilized. The dried water-soluble extract was dissolved in 600µl of standard and 10mM imidazole as pH indicator. NMR spectroscopy was performed on a 14.1T NMR spectrometer (Bruker Biospin, Billerica, MA), equipped with a cryoprobe and automatic sample changer. ^{1}H spectra were acquired as described previously and resonances were quantified using Chenomx NMR Suite (Chenomx Inc., Edmonton, Canada).

Tumor spheroid culture

LnCAP cells were trypsinized and diluted in a mixture of 1:1 (v/v) sodium alginate, BD Matrigel™ (Becton Dickinson, Oxford, UK) to a concentration of 1 x 10^5 cells/mL. For microscopy experiments, this mixture was loaded into a 1mL syringe and extruded through a 23G needle directly into a 100mM $CaCl_2$. For hyperpolarized experiments, cells at the same concentration were directly loaded into hollow fibers (A/G Technology Corporation, NY) and dropped into a 100mM $CaCl_2$ solution to polymerize. To ensure adequate oxygenation, spheroids were cultured in 6-well plates on a rotating incubator placed in a cell culture incubator. For viability studies, spheroids were stained with LIVE/DEAD Viability Kit (Thermo Scientific, MA) according to manufacturer's instructions. Histological and immunohistological staining were performed on spheroids that were fixed in 10% neutral buffered formalin and embedded in paraffin by the MSKCC Molecular Cytology Core Facility.

Hyperpolarization and magnetic resonance spectroscopy

[1-^{13}C] pyruvate was prepared for HP according to published reports (16) using a prototype SpinLab (General Electric, Niskayuna, New York, USA) for approximately 90 min before dissolving with a 40mM Tris buffer.

NMR studies were performed on a 1 Tesla Magritek Spectrometer (Magritek, San Diego, CA) using a 5mm ^{1}H/^{13}C coil. The dissolution process, transfer and transit to spectrometer was approximately 20s. Hollow fibers filled with cancer cell spheroids were directly deposited in a 5mm NMR tube before injection of a solution of 10mM hyperpolarized [1-^{13}C] pyruvate. For the acquisition of spectra, a repetition time (TR) of 4s was applied for a total of 25 scans using a 10 degree flip angle. Quantification of NMR spectra was performed using Mnova NMR (Escondido, CA).

Results

Targeted AKT chemotherapy in PTEN-mutated prostate cancer cells results in growth inhibition

The mutational landscape of prostate cancer has been annotated in large-scale sequencing initiatives(17). Using the MSKCC cBioPortal for Cancer Genomics, a web resource for visualizing cancer genomics data(18), mutations in the PAM pathway account for 29% of 333 sequenced patients with prostate adenocarcinoma. Of these, 21% of patients had mutations in the *PTEN* gene that codes for a phosphatase that acts as a negative regulator to AKT. The two next frequent mutations occur upstream of AKT, with PI3K regulatory subunit alpha (*PIK3R1* gene) accounting for 7% of mutations and the gene encoding for the catalytic subunit alpha (*PIK3CA*) accounting for another 7% (**Figure 1A**). Informed by these mutations, we first investigated the ability of AKT inhibitors to inhibit growth of prostate cancer cell lines.

Using MK2206, a non-ATP competitive inhibitor that has been trialled in patients(19), a dose-escalation study performed on PTEN-mutated LnCAP cells (**Figure 1B**) with a 50% reduction in growth seen at 1uM MK2206. At this concentration, AKT activity is inhibited as early as 2 hr post-treatment, evidenced by loss of phosphorylation of AKT at residue Ser473. This loss of AKT is sustained in both PC3 and LnCAP cell lines over a period of 24 hr (**Figure 1C**).

Similar growth inhibitory effects are seen with two other AKT inhibitors, perifosine and GDC-0068 on LnCAP and PC3 cells (homozygous *PTEN*-deleted). Although perifosine and MK2206 are non-ATP competitive inhibitors of AKT while GDC-0068 is ATP-competitive, a growth inhibitory effect was evident for both cell lines detected at the concentrations shown in **Figure 1D**.

MK2206 treatment reduces cell motility and aerobic glycolysis, independent of changes in ATP/ADP ratio

Activation of AKT requires recruitment of the kinase to the plasma membrane(2). Accordingly, MK2206 inhibition results in a dramatic reduction of AKT localization to the cell membrane as evidenced by immunofluorescence using a p-AKT (Ser473) primary antibody as shown in **Figure 2A**. Recently, AKT recruitment to the plasma membrane has been

shown to rely on components of the cytoskeleton, in an energy-requiring process(20). To our surprise, 1μM of MK2206, while sufficient to block activation of AKT, resulted in no change to the ratio of ADP/ATP in the cell. As a positive control, 5mM of the glucose analog, 2-deoxyglucose (2-DG) resulted in a significant increase in the ADP/ATP ratio, from a control value of 0.03 ± 0.01 to 0.13 ± 0.03, $p<0.05$ (**Figure 2B**).

While the ratio of high-energy phosphates in the cell appeared to not significantly change after AKT inhibition, we observed a significant decrease in cell motility as well as metabolism. Cell-tracking experiments performed over a period of 6 hr on LnCAP cells treated with MK2206 revealed a decrease in motility from 0.72 ± 0.04 to 0.46 ± 0.03 μm/s, $p<0.05$ as shown in **Figure 2C**. Additionally, cellular metabolism was also altered, with both LnCAP and PC3 cells showing significantly decreased lactate secretion and glucose consumption, as evidenced by quantification of metabolites in cell culture media (**Figure 2D**).

Isotopic tracing experiments using [1,6-$^{13}C_2$] glucose revealed that the change in metabolism could be ascribed to reduced aerobic glycolysis. While vehicle (DMSO) treated LnCAP cells demonstrated no significance in ^{13}C-fractional enrichment in both alanine and lactate compared to untreated cells, MK2206-treated cells showed decreased fractional enrichment in both these metabolites. Alanine levels in the media of DMSO-treated cells were enriched to 31.6 ± 13.0 compared to MK2206-treated cells at 14.7 ± 4.0 %, $p<0.05$ (**Figure 2E**). Alanine enrichment from ^{13}C-labeled glucose can be attributed to alanine transaminase activity that converts glucose-derived pyruvate to alanine(21). A similar trend was observed with lactate (79.3 ± 13.0 vs. 37.6 ±10.0 %, DMSO vs. MK2206, $p<0.05$), as shown in **Figure 2F**. Collectively, these changes in metabolism can be attributed to a reduced rate of aerobic glycolysis in LnCAP cells 24 hr after treatment with MK2206. To determine the mechanism behind reduced glycolysis, we quantified the NAD^+/NADH ratio in cells and MK2206-treated cells had a lower ratio of co-factors compared to vehicle-treated cells (0.799 ± 0.107 vs. 0.988 ± 0.162, $p<0.05$) (**Figure 2G and Supp. Figure 1**).

Measurement of a number of transporters and enzymes linked to metabolism through western blotting did not reveal significant changes in total protein levels (**Supp. Figure 2**). Similarly, there was no significant localization of hexokinase II (HKII) or glucose transporter 1 (Glut-1) in LnCAP cells after treatment with MK2206 (**Supp. Figure 3** and **Supp. Figure 4**, respectively).

LnCAP cells grown in alginate:Matrigel assemble into tumor spheroids that metabolize hyperpolarized [1-^{13}C] pyruvate

The reduction of aerobic glycolysis suggested that hyperpolarized MRS may be able to detect MK2206-induced AKT inhibition. The ability to rapidly measure metabolism in biopsy-acquired tissues may allow an additional biomarker for evaluating tumor grade and/or tumor treatment response. To better mimic human disease, we wanted to perform hyperpolarized experiments on 3D tumor spheroids.

Using a matrix of 1:1 sodium alginate:Matrigel, LnCAP cells rapidly self-assemble into 3D spheroid structures over a period of 24 hr as visualized using time-lapse microscopy in **Supp. Figure 5**. These spheroids are randomly distributed when visualized under light microscopy (**Figure 3A**, left panel), contain many DAPI-stained nuclei (**Figure 3A**, middle panel) and calcein-AM, a fluorescent marker of cell viability showed that these structures were predominantly viable (**Figure 3A**, right panel). These spheroids have a distribution of sizes that peaks at a cross-section of 200µm (**Figure 3B**).

For hyperpolarized experiments, the alginate:Matrigel matrix seeded with LnCAP cells were deposited into porous hollow fibers, as depicted in **Figure 3C**. The porous fibers allow gaseous and metabolite exchange, providing for extended culture periods. Direct deposition of the hollow fiber in a 5mm NMR tube followed by injection of 5mM HP [1-^{13}C] pyruvate resulted in rapid formation of [1-^{13}C] lactate (**Figure 3D**).

Besides spheroid culture, alginate:Matrigel threads containing high concentrations of LnCAP cells that mimicked dimensions of human biopsies were also tested. In contrast to distinct spheroids, these threads had evenly dispersed cells throughout the structure. These threads can be wound around a custom-printed insert built to fit into a 5mm NMR. Injection of a HP [1-13C] pyruvic acid solution to the threads also resulted in the formation of [1-13C] lactate (**Supp. Figure 6**). These 'biopsy mimics' represent another potential utility of hyperpolarized pyruvate in human samples. Patient-derived material can be directly deposited into an NMR tube without further manipulation and can then be retrieved for downstream analysis

Targeted AKT inhibitor treatment tumor spheroids reduces hyperpolarized [1-^{13}C] pyruvic acid conversion to [1-^{13}C] lactate

Having demonstrated the ability to grow tumor spheroids in NMR-compatible scaffolds, we went on to investigate if HP MRS can be used to detect metabolic changes associated with AKT inhibition. LnCAP spheroids grown in hollow-fiber scaffolds were deposited into an NMR tube immediately before dissolution of a HP pyruvate sample. In vehicle-treated threads, HP pyruvate was robustly converted to lactate. However, treatment with MK2206 rapidly reduces the rate of lactate formation (**Figure 4A**). Quantification of the amount of lactate produced as a ratio of pyruvate hydrate in MK2206-treated threads revealed a reduction of approximately one-third compared to DMSO-treated threads (0.08 ± 0.006 vs. 0.29 ± 0.012, $p<0.05$) as evidenced in **Figure 4B**. On-target inhibition in these threads was confirmed using immunohistochemistry with p-AKT (Ser473) primary antibody (**Figure 4C**). Activated AKT in vehicle-treated spheroids were concentrated on the plasma membrane of spheroids and this staining pattern was lost after drug treatment. Further immunohistochemical staining of these spheroids showed similar amounts of Ki-67 staining between vehicle and MK2206 treatment (31.7 ± 2.5 vs. 34.0 ± 1.7 %) that was not significantly different between the two samples ($p>0.05$) suggesting that at this early time-point, the number of proliferating cells in the sets of spheroids were similar (**Figures 4D and 4E**).

Discussion

The vast majority of prostate cancer patients that present with localized disease at diagnosis are treated with surgical resection and have an excellent prognosis(22). However, about a third of treated patients present with recurrent disease and are then put on to androgen deprivation therapy. While patients typically exhibit an early response to androgen deprivation, the majority of patients then develop androgen resistance(23), leading to castration-resistant prostate cancer (CRPC). Previous large-scale sequencing studies have found mutations in the PAM pathway in 42% of localized disease and 100% of advanced disease, suggesting that this pathway plays a critical role in CRPC(24).

This has led to a number of clinical trials involving inhibitors of different components of this pathway. In general, these drugs fall into 4 broad classes(25), PI3K inhibitors, AKT inhibitors, allosteric and ATP-site mTOR inhibitors and dual PI3K/mTOR inhibitors, although none are yet approved for use in prostate cancer. One of the biggest challenges of targeting the PAM pathway has been the lack of companion biomarkers that can identify patient response(26). The majority of clinical biomarkers have been histology-based, for example, the phosphorylation of ribosomal protein S6 (p-S6) in pre-treatment compared with post-treatment biopsies(27). However, the same study found no association between p-S6 staining in biopsies with tumor proliferation and apoptosis.

The possibility of using HP-MRS to detect changes in metabolism as a potential biomarker for on-target therapeutic inhibition motivated this study. We selected AKT inhibitors as this kinase have been called the master regulator of aerobic glycolysis(28) and has been shown to regulate glucose transporters(29), hexokinase(30) as well as phosphofructokinase(31). Our experiments support these observations, with both PC3 and LnCAP cells, that are sensitive to growth inhibition by the AKT inhibitor, MK2206, demonstrating reduced lactate secretion and glucose consumption. These metabolic changes occur rapidly, before any change in cell viability. We also saw a change in cell velocity, consistent with previous work using PI3K/AKT inhibitors that show reduced motility in endometrial cancer(32), glioblastoma(33) and breast cancer(34). The reduction in aerobic glycolysis and cell motility was not accompanied by changes in cellular ADP/ATP ratios. Cellular high-energy phosphate levels are tightly regulated, with increased ADP and AMP concentrations activating AMP-activated protein kinase (AMPK)(35). AMPK phosphorylates diverse downstream targets that can lead to autophagy, mitophagy, cell cycle arrest as well as the termination of protein synthesis(36). We postulate that changes in nutrient consumption (such as aerobic glycolysis) and cellular motility are early, reversible events in response to AKT inhibition while depletion of ATP occur later with a myriad of downstream consequences that are irreversible and therefore energetically costly. As such, the metabolic changes we observe using 1μM MK2206, 24 hr post-treatment, may represent an acute response of LnCAP cells to AKT inhibition, preceding the growth-inhibitory effects of the drug that occur at later time points. The molecular mechanisms that govern these metabolic changes will be the focus of future studies as our results have shown that reduced aerobic glycolysis is not accompanied by relocalization and/or reduced total protein levels of transporters and enzymes involved in metabolism. It is likely that at early time-points, such as 24 hr post-AKT inhibition, changes in the affinity of enzymes and transporters involved in metabolism might account for the changes seen in nutrient consumption.

We have demonstrated the ability to measure metabolism in cancer spheroids using HP [1-^{13}C] pyruvate. While previous studies have demonstrated the ability to measure metabolism in cells that were grown *ex situ*, pioneering experiments utilized either suspension cells or trypsinized, adherent cell suspensions. The majority of cells derived from vertebrates are anchorage-dependent and trypsinization has been shown to change cell physiology(37). As such, more sophisticated models of culture suited for HP NMR studies have been developed including using microcarriers(38) as well as sodium alginate beads(13). Subsequent experiments have also been performed on whole organs such as the perfused heart(39) and liver(40). The techniques described in this study add another pre-clinical cellular model that can be interrogated using HP-MRS. As a proof-of-concept, hyperpolarized experiments were carried out on immortalized cell-line derived spheroids, but we expect that patient-derived organoids can also be used in the future for similar studies. While culturing patient-derived

organoids can be technically challenging and costly(41), there are many advantages to this 3D culture system and the non-destructive nature of HP-MRS means that these precious samples can be retrieved for downstream applications. Current organoid culture methods use extracellular matrices that are similar to the one utilized in this study and the fidelity of organoid culture to clinical disease may prove informative in complementing clinical trials of HP-MRS. There are a number of on-going clinical trials of using hyperpolarized pyruvate as a biomarker of response post-chemotherapy in prostate (ClinicalTrials.gov Identifier: NCT02911467) as well as breast cancer (NCT03121989) patients. The ability to perform hyperpolarized experiments on patient-derived organoids with similar genomic and molecular characteristics as clinical trial participants will be invaluable. As organoids can be continually cultured and can be treated with a variety of chemotherapies, HP-MRS experiments performed on organoids can ultimately be used to predict patient populations that will most benefit from this imaging method.

In summary, this study has shown that targeted AKT inhibition in prostate cancer cells result in a reduction of cell growth. This growth inhibitory effect is preceded by changes in cell metabolism, measurable as a decrease in aerobic glycolysis. HP-MRS can be used to detect AKT inhibition in 3D cell spheroid models. The methods described here can be translated to patient-derived organoids, with the possibility of informing future imaging clinical trials.

Acknowledgements

The authors would like to extend their appreciation to members of the Neal Rosen lab for their helpful discussions and suggestions for experiments.

Figure Legends

FIGURE 1. The PI3K/AKT/mTOR pathway is frequently mutated in prostate cancer and can be targeted using AKT inhibitors. (**A**) Genomic sequencing data from 333 patients with prostate adenocarcinoma showcasing mutations in 7 genes in the PI3K/AKT/mTOR pathway, detectable in 29% of all patients. (**B**) Growth curves of LnCAP cells treated with increasing concentrations of non-ATP competitive AKT inhibitor, MK2206. (**C**) Western blots of LnCAP and PC3 cells after treatment with MK2206 reveal rapid and sustained inhibition of AKT signaling as evidenced by loss of p-AKT (S473) phosphorylation. (**D**) PTEN null cells (LnCAP and PC3) are sensitive to growth inhibition by different classes of AKT inhibitors, including MK2206, perifosine and GDC0068

FIGURE 2. AKT inhibition in LnCAP cells results in reduced cell motility and aerobic glycolysis. (**A**) Vehicle-treated (DMSO) LnCAP cells concentrate p-AKT (S473) at the

plasma membrane (left panel) and staining is lost 24 hr after treatment with MK2206 (right panel). (**B**) Measurement of ADP/ATP ratio in MK2206-treated cells were not significantly different from control cells, as opposed to treatment using a glycolytic inhibitor, 2-deoxyglucose (2-DG). (**C**) Representative images of LnCAP cells used to quantify velocity, with AKT inhibition resulting in significantly reduced cell motility. (**D**) Quantification of metabolites in culture media in LnCAP and PC3 cells 24 hr after treatment with MK2206 reveal reduced lactate production and decreased glucose consumption. (**E**) and (**F**), Fractional enrichment experiments using [1,6-$^{13}C_2$] glucose in MK2206-treated cells result in a lower percentage of labeled lactate and alanine. (G) Quantification of co-factor ratios in LnCAP cells treated either with MK2206 or DMSO demonstrated lower ratios of NAD^+/NADH 24 hr post-treatment.

FIGURE 3. LnCAP cells form 3D-spheroids in extracellular matrix that are amenable to hyperpolarized magnetic resonance spectroscopy. (**A**) LnCAP cells grown in 1:1 alginate:Matrigel form distinct organoids as visualized under light microscopy (left panel), that contain multiple DAPI-stained nuclei (middle panel) and stain positive with calcein-AM, a fluorescent marker of cell viability (right panel). (**B**) Spheroid cross-section distribution peaks at approximately 200μm. (**C**) For hyperpolarized experiments, LnCAP cells seeded in matrix were deposited into porous hollow fibers, (**D**) Direct deposition of the hollow fiber in a 5mm NMR tube followed by injection of 5mM HP [1-^{13}C] pyruvate resulted in rapid formation of [1-^{13}C] lactate.

FIGURE 4. Hyperpolarized magnetic resonance spectroscopy of LnCAP spheroids reveal reduced lactate production post AKT inhibition. (**A**) Representative spectra of spheroids treated with either DMSO or MK2206 after 24 hr. A total of 25 spectra were acquired with a 10° flip angle every 4 s after delivery of approximately 1mM hyperpolarized [1-^{13}C] pyruvate. * is an unidentified contaminant that is present in the dissolution. (**B**), Quantification of the summed lactate integral divided by the integral of the lactate and pyruvate hydrate in MK2206 treated spheroids were significantly lower than vehicle treatment. (**C**) Immunohistochemistry using a primary antibody against p-AKT (Ser473) showed significantly reduced AKT phosphorylation 24 hr after MK2206 treatment with (**D**) no significant change in Ki-67 as quantified in (**E**).

References

1. Chen Y, Scher HI. Prostate cancer in 2011: Hitting old targets better and identifying new targets. Nature reviews Clinical oncology 2012;9(2):70-72.
2. Martini M, De Santis MC, Braccini L, Gulluni F, Hirsch E. PI3K/AKT signaling pathway and cancer: an updated review. Ann Med 2014;46(6):372-383.
3. Cully M, You H, Levine AJ, Mak TW. Beyond PTEN mutations: the PI3K pathway as an integrator of multiple inputs during tumorigenesis. Nature Reviews Cancer 2006;6(3):184-192.
4. Chalhoub N, Baker SJ. PTEN and the PI3-kinase pathway in cancer. Annu Rev Pathol 2009;4:127-150.
5. Taylor BS, Schultz N, Hieronymus H, Gopalan A, Xiao Y, Carver BS, Arora VK, Kaushik P, Cerami E, Reva B, Antipin Y, Mitsiades N, Landers T, Dolgalev I, Major JE, Wilson M, Socci ND, Lash AE, Heguy A, Eastham JA, Scher HI, Reuter VE, Scardino PT, Sander C, Sawyers CL, Gerald WL. Integrative genomic profiling of human prostate cancer. Cancer cell 2010;18(1):11-22.
6. Bitting RL, Armstrong AJ. Targeting the PI3K/Akt/mTOR pathway in castration-resistant prostate cancer. Endocrine-related cancer 2013;20(3):R83-99.
7. Brindle K. New approaches for imaging tumour responses to treatment. Nature reviews Cancer 2008;8(2):94-107.
8. Tee SS, Keshari KR. Novel Approaches to Imaging Tumor Metabolism. Cancer journal 2015;21(3):165-173.
9. Ardenkjaer-Larsen JH, Fridlund B, Gram A, Hansson G, Hansson L, Lerche MH, Servin R, Thaning M, Golman K. Increase in signal-to-noise ratio of > 10,000 times in liquid-state NMR. Proceedings of the National Academy of Sciences of the United States of America 2003;100(18):10158-10163.
10. Nelson SJ, Kurhanewicz J, Vigneron DB, Larson PEZ, Harzstark AL, Ferrone M, van Criekinge M, Chang JW, Bok R, Park I, Reed G, Carvajal L, Small EJ, Munster P, Weinberg VK, Ardenkjaer-Larsen JH, Chen AP, Hurd RE, Odegardstuen LI, Robb FJ, Tropp J, Murray JA. Metabolic Imaging of Patients with Prostate Cancer Using Hyperpolarized [1-C-13]Pyruvate. Sci Transl Med 2013;5(198).
11. Gillies RJ, Mackenzie NE, Dale BE. Analyses of Bioreactor Performance by Nuclear Magnetic-Resonance Spectroscopy. Bio-Technol 1989;7(1):50-54.
12. Day SE, Kettunen MI, Gallagher FA, Hu DE, Lerche M, Wolber J, Golman K, Ardenkjaer-Larsen JH, Brindle KM. Detecting tumor response to treatment using hyperpolarized C-13 magnetic resonance imaging and spectroscopy. Nat Med 2007;13(11):1382-1387.
13. Keshari KR, Kurhanewicz J, Jeffries RE, Wilson DM, Dewar BJ, Van Criekinge M, Zierhut M, Vigneron DB, Macdonald JM. Hyperpolarized C-13 Spectroscopy and an NMR-Compatible Bioreactor System for the Investigation of Real-Time Cellular Metabolism. Magnetic Resonance in Medicine 2010;63(2):322-329.
14. Fatehullah A, Tan SH, Barker N. Organoids as an in vitro model of human development and disease. Nat Cell Biol 2016;18(3):246-254.
15. Gao D, Vela I, Sboner A, Iaquinta PJ, Karthaus WR, Gopalan A, Dowling C, Wanjala JN, Undvall EA, Arora VK, Wongvipat J, Kossai M, Ramazanoglu S, Barboza LP, Di W, Cao Z, Zhang QF, Sirota I, Ran L, MacDonald TY, Beltran H, Mosquera JM, Touijer KA, Scardino PT, Laudone VP, Curtis KR, Rathkopf DE, Morris MJ, Danila DC, Slovin SF, Solomon SB, Eastham JA, Chi P, Carver B, Rubin MA, Scher HI, Clevers H, Sawyers CL, Chen Y. Organoid cultures derived from patients with advanced prostate cancer. Cell 2014;159(1):176-187.
16. Keshari KR, Sriram R, Koelsch BL, Van Criekinge M, Wilson DM, Kurhanewicz J, Wang ZJ. Hyperpolarized 13C-pyruvate magnetic resonance reveals rapid lactate export in metastatic renal cell carcinomas. Cancer research 2013;73(2):529-538.
17. Robinson D, Van Allen EM, Wu YM, Schultz N, Lonigro RJ, Mosquera JM, Montgomery B, Taplin ME, Pritchard CC, Attard G, Beltran H, Abida W, Bradley RK, Vinson J, Cao X, Vats P, Kunju LP, Hussain M, Feng FY, Tomlins SA, Cooney KA, Smith DC, Brennan C, Siddiqui J,

Mehra R, Chen Y, Rathkopf DE, Morris MJ, Solomon SB, Durack JC, Reuter VE, Gopalan A, Gao J, Loda M, Lis RT, Bowden M, Balk SP, Gaviola G, Sougnez C, Gupta M, Yu EY, Mostaghel EA, Cheng HH, Mulcahy H, True LD, Plymate SR, Dvinge H, Ferraldeschi R, Flohr P, Miranda S, Zafeiriou Z, Tunariu N, Mateo J, Perez-Lopez R, Demichelis F, Robinson BD, Schiffman M, Nanus DM, Tagawa ST, Sigaras A, Eng KW, Elemento O, Sboner A, Heath EI, Scher HI, Pienta KJ, Kantoff P, de Bono JS, Rubin MA, Nelson PS, Garraway LA, Sawyers CL, Chinnaiyan AM. Integrative clinical genomics of advanced prostate cancer. Cell 2015;161(5):1215-1228.

18. Gao JJ, Aksoy BA, Dogrusoz U, Dresdner G, Gross B, Sumer SO, Sun YC, Jacobsen A, Sinha R, Larsson E, Cerami E, Sander C, Schultz N. Integrative Analysis of Complex Cancer Genomics and Clinical Profiles Using the cBioPortal. Sci Signal 2013;6(269).
19. Yap TA, Yan L, Patnaik A, Fearen I, Olmos D, Papadopoulos K, Baird RD, Delgado L, Taylor A, Lupinacci L, Riisnaes R, Pope LL, Heaton SP, Thomas G, Garrett MD, Sullivan DM, de Bono JS, Tolcher AW. First-in-man clinical trial of the oral pan-AKT inhibitor MK-2206 in patients with advanced solid tumors. J Clin Oncol 2011;29(35):4688-4695.
20. Zhao Y, Lin YT, Zhang HH, Manas A, Tang WW, Zhang YZ, Wu DQ, Lin AN, Xiang JL. Ubl4A is required for insulin-induced Akt plasma membrane translocation through promotion of Arp2/3-dependent actin branching. Proceedings of the National Academy of Sciences of the United States of America 2015;112(31):9644-9649.
21. Damico LA, White LT, Yu X, Lewandowski ED. Chemical versus isotopic equilibrium and the metabolic fate of glycolytic end products in the heart. J Mol Cell Cardiol 1996;28(5):989-999.
22. Siegel R, DeSantis C, Virgo K, Stein K, Mariotto A, Smith T, Cooper D, Gansler T, Lerro C, Fedewa S, Lin CC, Leach C, Cannady RS, Cho HS, Scoppa S, Hachey M, Kirch R, Jemal A, Ward E. Cancer treatment and survivorship statistics, 2012. Ca-Cancer J Clin 2012;62(4):220-241.
23. Walsh PC. Re: The Natural History of Metastatic Progression in Men with Prostate-Specific Antigen Recurrence After Radical Prostatectomy: Long-Term Follow-up Editorial Comment. J Urology 2012;188(3):809-809.
24. Taylor BS, Schultz N, Hieronymus H, Gopalan A, Xiao YH, Carver BS, Arora VK, Kaushik P, Cerami E, Reva B, Antipin Y, Mitsiades N, Landers T, Dolgalev I, Major JE, Wilson M, Socci ND, Lash AE, Heguy A, Eastham JA, Scher HI, Reuter VE, Scardino PT, Sander C, Sawyers CL, Gerald WL. Integrative Genomic Profiling of Human Prostate Cancer. Cancer Cell 2010;18(1):11-22.
25. Fruman DA, Rommel C. PI3K and cancer: lessons, challenges and opportunities. Nat Rev Drug Discov 2014;13(2):140-156.
26. Edlind MP, Hsieh AC. PI3K-AKT-mTOR signaling in prostate cancer progression and androgen deprivation therapy resistance. Asian J Androl 2014;16(3):378-386.
27. Armstrong AJ, Netto GJ, Rudek MA, Halabi S, Wood DP, Creel PA, Mundy K, Davis SL, Wang T, Albadine R, Schultz L, Partin AW, Jimeno A, Fedor H, Febbo PG, George DJ, Gurganus R, De Marzo AM, Carducci MA. A Pharmacodynamic Study of Rapamycin in Men with Intermediate- to High-Risk Localized Prostate Cancer. Clin Cancer Res 2010;16(11):3057-3066.
28. Mosca E, Alfieri R, Maj C, Bevilacqua A, Canti G, Milanesi L. Computational modeling of the metabolic states regulated by the kinase Akt. Front Physiol 2012;3.
29. Kim DI, Lim SK, Park MJ, Han HJ, Kim GY, Park SH. The involvement of phosphatidylinositol 3-kinase/Akt signaling in high glucose-induced downregulation of GLUT-1 expression in ARPE cells. Life Sci 2007;80(7):626-632.
30. Miyamoto S, Murphy AN, Brown JH. Akt mediates mitochondrial protection in cardiomyocytes through phosphorylation of mitochondrial hexokinase-II. Cell Death Differ 2008;15(3):521-529.
31. Deprez J, Vertommen D, Alessi DR, Hue L, Rider MH. Phosphorylation and activation of heart 6-phosphofructo-2-kinase by protein kinase B and other protein kinases of the insulin signaling cascades. J Biol Chem 1997;272(28):17269-17275.
32. Winder A, Unno K, Yu Y, Lurain J, Kim JJ. The allosteric AKT inhibitor, MK2206, decreases tumor growth and invasion in patient derived xenografts of endometrial cancer. Cancer Biol Ther 2017:0.

33. Kwiatkowska A, Kijewska M, Lipko M, Hibner U, Kaminska B. Downregulation of Akt and FAK phosphorylation reduces invasion of glioblastoma cells by impairment of MT1-MMP shuttling to lamellipodia and downregulates MMPs expression. Bba-Mol Cell Res 2011;1813(5):655-667.
34. Choi JA, Jung YS, Kim JY, Kim HM, Lim IK. Inhibition of breast cancer invasion by TIS21/BTG2/Pc3-Akt1-Sp1-Nox4 pathway targeting actin nucleators, mDia genes. Oncogene 2016;35(1):83-93.
35. Hardie DG. AMP-activated protein kinase-an energy sensor that regulates all aspects of cell function. Gene Dev 2011;25(18):1895-1908.
36. Hardie DG, Ross FA, Hawley SA. AMPK: a nutrient and energy sensor that maintains energy homeostasis. Nat Rev Mol Cell Bio 2012;13(4):251-262.
37. Huang HL, Hsing HW, Lai TC, Chen YW, Lee TR, Chan HT, Lyu PC, Wu CL, Lu YC, Lin ST, Lin CW, Lai CH, Chang HT, Chou HC, Chan HL. Trypsin-induced proteome alteration during cell subculture in mammalian cells. J Biomed Sci 2010;17:36.
38. Gallagher FA, Kettunen MI, Day SE, Lerche M, Brindle KM. 13C MR spectroscopy measurements of glutaminase activity in human hepatocellular carcinoma cells using hyperpolarized 13C-labeled glutamine. Magn Reson Med 2008;60(2):253-257.
39. Schroeder MA, Atherton HJ, Ball DR, Cole MA, Heather LC, Griffin JL, Clarke K, Radda GK, Tyler DJ. Real-time assessment of Krebs cycle metabolism using hyperpolarized C-13 magnetic resonance spectroscopy. Faseb J 2009;23(8):2529-2538.
40. Moreno KX, Moore CL, Burgess SC, Sherry AD, Malloy CR, Merritt ME. Production of hyperpolarized 13CO2 from [1-13C]pyruvate in perfused liver does reflect total anaplerosis but is not a reliable biomarker of glucose production. Metabolomics 2015;11(5):1144-1156.
41. Weeber F, Ooft SN, Dijkstra KK, Voest EE. Tumor Organoids as a Pre-clinical Cancer Model for Drug Discovery. Cell Chem Biol 2017;24(9):1092-1100.

Figure 1

A

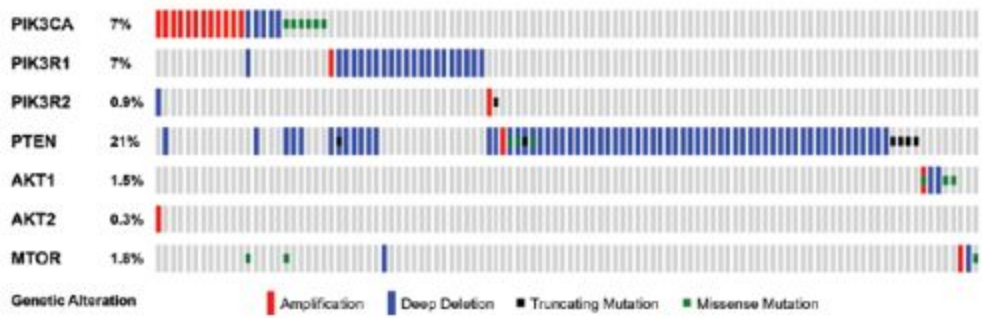

B

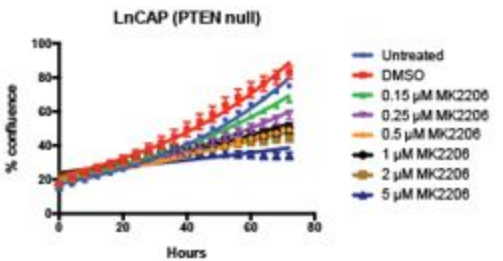

C

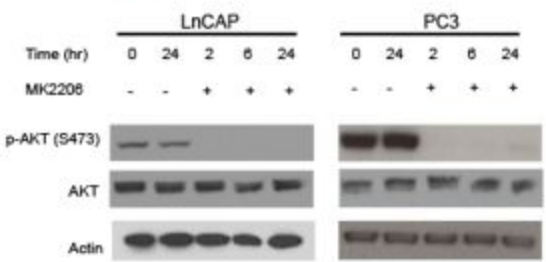

D

	$IC_{50(Confluence)}$			
	MK2206	Perifosine	GDC0068	PTEN status
LnCAP	1μM	2μM	1μM	One mutated, one deleted allele
PC3	1μM	3μM	1μM	Homozygous deletion

Figure 2

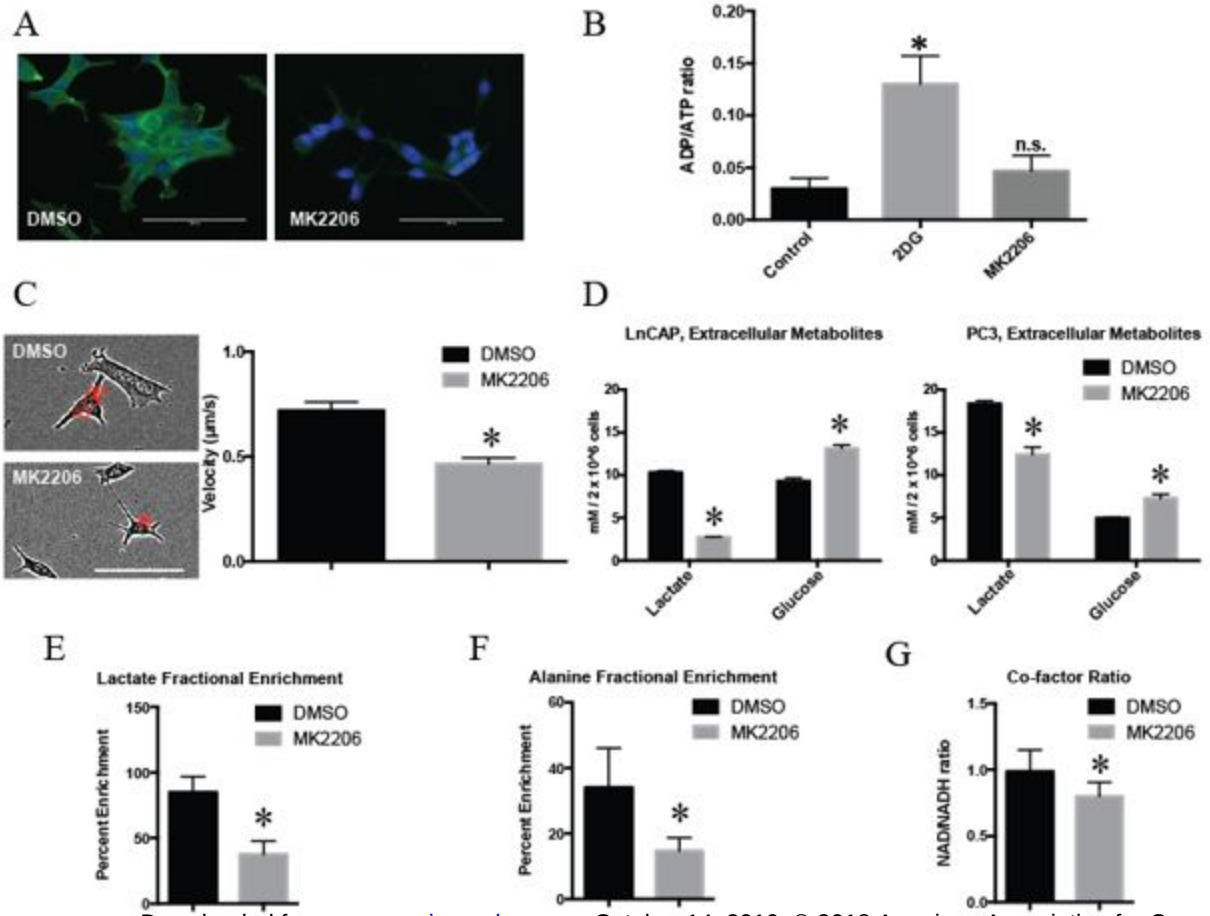

Figure 3

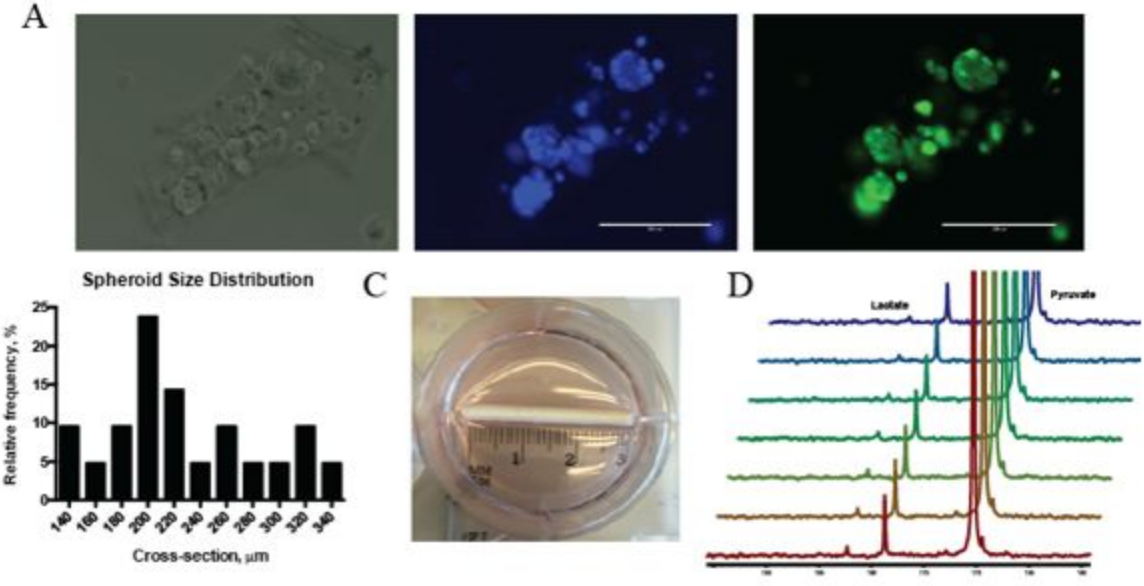

Figure 4

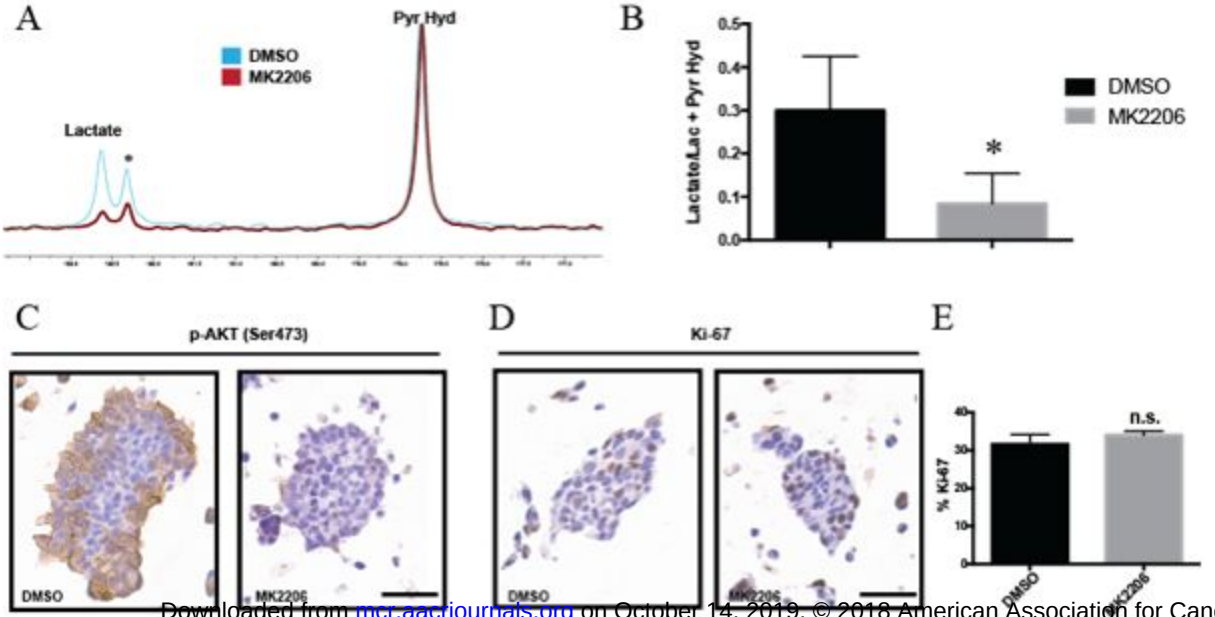

AACR American Association for Cancer Research

Molecular Cancer Research

Targeted AKT inhibition in prostate cancer cells and spheroids reduces aerobic glycolysis and generation of hyperpolarized [1-^{13}C] lactate

Sui Seng Tee, Izabela Suster, Steven Truong, et al.

Mol Cancer Res Published OnlineFirst January 12, 2018.